Available online at www.sciencedirect.com
ScienceDirect
International Journal of Heat and Mass Transfer 50 (2007) 181–187
International Journal of HEAT and MASS TRANSFER
www.elsevier.com/locate/ijhmt

# Non-similar solution of an unsteady mixed convection flow over a vertical cone with suction or injection

S. Roy [a,*], Prabal Datta [b], N.C. Mahanti [b]

[a] Department of Mathematics, Indian Institute of Technology Madras, Chennai 600 036, India
[b] Department of Applied Mathematics, B.I.T Mesra, Ranchi-835215, India

Received 1 December 2005; received in revised form 19 June 2006
Available online 6 September 2006

**Abstract**

Non-similar solution of an unsteady mixed convection flow over a vertical cone in the presence of surface mass transfer has been obtained when the axis of the cone is inline with the flow. The time dependent free stream velocity varying arbitrarily with time introduces unsteadiness in the flow field. The results have been obtained for accelerating and decelerating free stream velocities. The numerical difficulties arising at the starting point of the stream wise coordinate and for time dependent flow field are overcome by applying an implicit finite difference scheme in combination with the quasilinearization technique. Numerical results are reported here to account the effects of Prandtl number, buoyancy and mass transfer (injection and suction) parameters at different streamwise locations for various times on velocity and temperature profiles, and skin friction and heat transfer coefficients.


## 1. Introduction

In many practical circumstances unsteady mixed convection flows do not necessarily admit similarity solution and during the last two decades, a wide range of problems have appeared that demand detailed analysis of unsteady mixed convection flows which necessitates taking non-similarity into account. The unsteadiness and non-similarity in such flows may be due to free stream velocity or due to curvature of the body or due to surface mass transfer (suction or injection), or even possibly due to all these effects. The inherent mathematical difficulties involved in obtaining non-similar solutions for such problem enforced most investigators to confine their studies either to steady non-similar flows or to unsteady semi-similar or self-similar flows [1–7].

Convective heat transfer in unsteady flows over a stationary cone is important for the thermal design of various types of industrial equipments such as heat exchanger, conisters for nuclear waste disposal, nuclear reactor cooling system and geothermal reservoirs etc. In an early study, Heiring and Grosh [1] investigated the practical case of steady mixed convection from a vertical cone for $Pr = 0.7$. They made use of a similarity transformation which shows $(\frac{Gr_x}{Re_x^2})$ is the dominant dimensionless parameter that would categories the three regions, namely forced, free and mixed convection. In a further study, Himasekhar et al. [2] found the similarity solution of the mixed convection flow over a vertical rotating cone in an ambient fluid for a wide range of Prandtl numbers. Wang [3] has obtained a similarity solution of boundary layer flows on rotating cone, discs and axi-symmetric bodies with concentrated heat sources. In recent studies, Anilkumar and Roy [4], and Roy and Anilkumar [5] have presented, respectively, self-similar and semi-similar solutions of unsteady mixed convection flows from a rotating cone in a rotating fluid. In contrast, Kumari et al. [6] and Yih [7] have presented non-similar solutions to study the heat transfer characteristics in unsteady mixed convection flows from a vertical cone without and with porous media, respectively.

* Corresponding author. Fax: +91 44 2257 8470.
*E-mail address:* sjroy@iitm.ac.in (S. Roy).

0017-9310/$ - see front matter © 2006 Elsevier Ltd. All rights reserved.
doi:10.1016/j.ijheatmasstransfer.2006.06.024

**Nomenclature**

| | |
|---|---|
| $A$ | surface mass transfer parameter |
| $C_f$ | local skin friction coefficient |
| $C_p$ | specific heat at constant pressure |
| $f$, $F$ | dimensionless stream function and axial velocity component, respectively |
| $g$ | acceleration due to gravity |
| $G$ | dimensionless temperature |
| $Gr_x$ | Grashof number |
| $k$ | thermal conductivity |
| $m$ | exponent in the power law variation of the free stream velocity |
| $Nu$ | local Nusselt number |
| $Pr$ | Prandtl number |
| $Re_x$ | Reynolds number |
| $t$, $t^*$ | dimensional and dimensionless times, respectively |
| $T$ | temperature |
| $u$ | axial velocity component |
| $U$ | free stream velocity component |
| $v$ | radial velocity component |
| $x$ | axial coordinate |
| $y$ | transverse coordinate |

*Greek symbols*

| | |
|---|---|
| $\beta$ | volumetric coefficient of thermal expansion |
| $\gamma$ | half angle of the vertical cone |
| $\epsilon$ | unsteady parameter |
| $\xi$ | similarity variable |
| $\eta$ | similarity variable |
| $\lambda$ | buoyancy parameter |
| $\mu$ | dynamic viscosity |
| $\nu$ | kinematic viscosity |
| $\rho$ | density |
| $\phi$ | function of $t^*$ |
| $\psi$ | stream function |

*Subscripts*

| | |
|---|---|
| e | condition at the edge of the boundary layer |
| i | initial condition |
| $w$, $\infty$ | conditions at the wall and infinity, respectively |
| $\xi$, $\eta$, $t^*$ | denote the partial derivatives w.r. to these variables, respectively |

In many practical problems, the flow could be unsteady due to time dependent free stream velocity and there are several transport processes with surface mass transfer (i.e., injection or suction) in industry where the buoyancy force arises from thermal diffusion caused by temperature gradient. Therefore as a step towards the eventual development on unsteady mixed convection flows, it is interesting as well as useful to investigate the combined effects of thermal diffusion and surface mass transfer on a vertical cone where the free stream velocity varies arbitrarily with time.

The objective of the present analysis is to obtain non-similar solution of an unsteady mixed convection flow over a vertical cone with surface mass transfer (injection or suction). Non-similar solutions are obtained numerically by solving a set of coupled non-linear partial differential equation using an implicit finite difference scheme in combination with the quasilinearization technique. Particular cases of the present results have been compared with those of Hering and Grosh [1], Himasekhar et al. [2], and Kumari et al. [6].

## 2. Analysis

Consider a vertical circular cone with a half angle $\gamma$ along which a forced flow moves parallel to the axis of the cone with free stream velocity $u_\infty$ and temperature $T_\infty$. The surface of the cone is at a uniform higher temperature $T_w$, i.e., $T_w > T_\infty$ and the forced flow is in upward direction. The streamwise coordinate $x$ is measured from the apex of the cone along it's generator, and the transverse coordinate $y$ is measured normal to it into the fluid, respectively (see Fig. 1). Thermo-physical properties of the fluid in the flow model are assumed to be constant except the density variations causing a body force term in the momen-

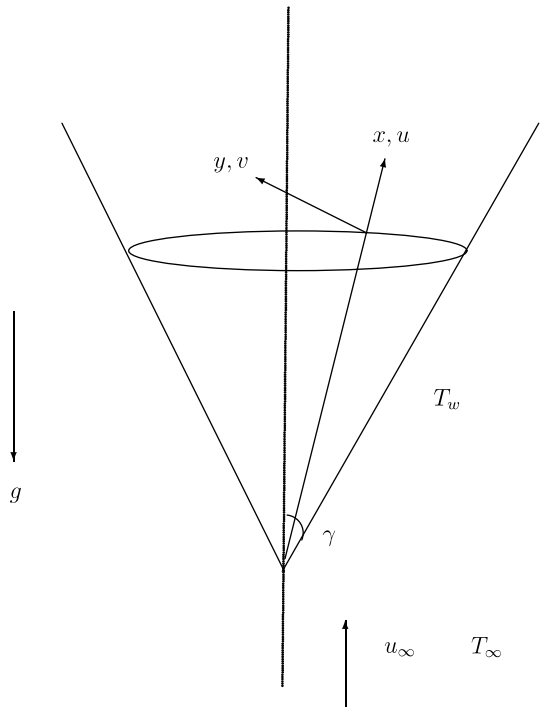


Fig. 1. Physical model and co-ordinate system.

tum equation. The Boussinesq approximation is invoked for the fluid properties to relate the density changes to temperature changes and to couple in this way the temperature field to the flow field. Under the above assumptions and imposing Mangler's transformation to reduce the axi-symmetric problem into a two-dimensional problem [8], the continuity, momentum and energy equations governing unsteady mixed convection flow along a vertical cone can be written as

$$\frac{\partial u}{\partial x}+\frac{\partial v}{\partial y}=0, \tag{1}$$

$$\frac{\partial u}{\partial t}+u\frac{\partial u}{\partial x}+v\frac{\partial u}{\partial y}=\frac{\partial u_e}{\partial t}+u_e\frac{\partial u_e}{\partial x}+v\frac{\partial^2 u}{\partial y^2}+g\beta\cos\gamma(T-T_\infty), \tag{2}$$

$$\frac{\partial T}{\partial t}+u\frac{\partial T}{\partial x}+v\frac{\partial T}{\partial y}=\frac{v}{Pr}\frac{\partial^2 T}{\partial y^2}. \tag{3}$$

The initial conditions are given by

$$u(x,y,0)=u_i(x,y),\quad v(x,y,0)=v_i(x,y),\quad T(x,y,0)=T_i(x,y). \tag{4}$$

The boundary conditions are given by

$$\begin{aligned}&u(x,0,t)=0,\quad v(x,0,t)=v_w(x),\\&T(x,0,t)=T_w=\text{Constant},\\&u(x,\infty,t)=u_e(x,t)=U(x)\phi(t^*)=u_\infty x^{m/3}\phi(t^*),\\&T(x,\infty,t)=T_\infty=\text{Constant}.\end{aligned} \tag{5}$$

Applying the following transformations:

$$\begin{aligned}&\eta=y\left(\frac{m+3}{6}\frac{U}{vx}\right)^{\frac{1}{2}},\quad \xi=\left(\frac{6}{m+3}\frac{vx}{U}\right)^{\frac{1}{2}},\\&t^*=\left(\frac{m+3}{6}\right)\frac{dU}{dx}t,\quad \psi(x,y,t)=\left(\frac{6}{m+3}vxU\right)^{\frac{1}{2}}\phi(t^*)f(\xi,\eta,t^*),\\&u=\frac{\partial\psi}{\partial y},\quad v=-\frac{\partial\psi}{\partial x},\quad f_\eta(\xi,\eta,t^*)=F(\xi,\eta,t^*),\\&u=U\phi(t^*)F(\xi,\eta,t^*),\\&v=-2^{-1}\left(\frac{6}{m+3}\frac{vU}{x}\right)^{1/2}\phi\left[\left(\frac{m+3}{3}\right)f+\xi f_\xi-\eta F\right.\\&\quad\left.+2\left(\frac{m-3}{3}\right)t^*\left\{\phi^{-1}\frac{d\phi}{dt^*}f+f_{t^*}\right\}\right],\\&G(\xi,\eta,t^*)=\frac{T-T_\infty}{T_w-T_\infty},\end{aligned} \tag{6}$$

to Eqs. (1)–(3), it is found that Eq. (1) is satisfied identically, and Eqs. (2) and (3) reduce to

$$\begin{aligned}&F_{\eta\eta}+\phi fF_\eta+\frac{2m}{m+3}\phi(1-F^2)+\frac{6}{m+3}\lambda\phi^{-1}G+\left[\phi^{-1}\frac{d\phi}{dt^*}(1-F)-F_{t^*}\right]\\&\quad+2\left(\frac{m-3}{m+3}\right)t^*\left[\frac{d\phi}{dt^*}(1-F^2+fF_\eta)+\phi(f_{t^*}F_\eta-FF_{t^*})\right]\\&\quad=\frac{3}{m+3}\phi\xi(FF_\xi-F_\eta f_\xi),\end{aligned} \tag{7}$$

$$\begin{aligned}&Pr^{-1}G_{\eta\eta}+\phi fG_\eta-G_{t^*}+2\left(\frac{m-3}{m+3}\right)t^*\left[\frac{d\phi}{dt^*}fG_\eta+\phi(f_{t^*}G_\eta-FG_{t^*})\right]\\&\quad=\xi(FG_\xi-G_\eta f_\xi),\end{aligned} \tag{8}$$

where

$$Pr=\frac{\mu C_p}{k},\quad Gr_x=\frac{g\beta x^3(T_w-T_\infty)\cos\gamma}{v^2},\quad Re_x=\frac{u_\infty x}{v}\ \text{ and }\ \lambda=\frac{Gr_x}{Re_x^2}.$$

It may be noted that for $m=\frac{3}{2}$, $\lambda$ becomes a constant and numerical solutions are computed for different values of $\lambda$ as discussed in Section 4.

Here $\xi$, $\eta$ are the transformed co-ordinates; $\eta_\infty$ is the edge of the boundary layer; $\psi$ and $f$ are dimensional and dimensionless stream functions, respectively; $F$ and $G$ are, respectively, dimensionless velocity and temperature.

The boundary conditions reduce to

$$\begin{aligned}&F(\xi,0,t^*)=0,\quad G(\xi,0,t^*)=1\quad\text{at }\eta=0,\\&F(\xi,\infty,t^*)=1,\quad G(\xi,\infty,t^*)=0\quad\text{as }\eta\to\infty,\end{aligned} \tag{9}$$

where $f=\int_0^\eta F d\eta+f_w$ and $f_w$ is given by

$$\begin{aligned}&\phi f_w+\left(\frac{m}{m+3}\right)\xi(f_\xi)_w+2\left(\frac{m-3}{m+3}\right)t^*\left[\frac{d\phi}{dt^*}f_w+\phi(f_{t^*})_w\right]\\&\quad=-\left(\frac{v_w}{v}\right)\xi=A\xi;\\&A=-\frac{v_w}{v}.\end{aligned}$$

The surface mass transfer parameter $A>0$ or $A<0$ according to whether there is a suction or injection. It is assumed that the flow is steady at time $t^*=0$ and becomes unsteady for $t^*>0$ due to the time dependent free stream velocity $u_e(x,t)=U(x)\phi(t^*)=u_\infty x^{m/3}\phi(t^*)$, where $\phi(t^*)=1+\epsilon t^{*2}$; $\epsilon>or<0$. Hence, the initial conditions (i.e., condition at $t^*=0$) are given by the steady state equations obtained from the Eqs. (7) and (8) by substituting $\phi(t^*)=1, \frac{d\phi}{dt^*}=F_{t^*}=G_{t^*}=0$ when $t^*=0$. It may be noted that the steady state equations with $\xi=0$, $\lambda=0$ and $m=0$ in the present problem are the same as those of Kumari et al. [6].

The quantities of physical interest are as follows [9,10]:

The local skin friction coefficient is given by

$$C_f=\frac{2\left[\mu\frac{\partial u}{\partial y}\right]_w}{\rho U^2}=2(Re_x)^{-\frac{1}{2}}\left(\frac{m+3}{6}\right)^{\frac{1}{2}}\phi(t^*)(F_\eta)_w.$$

Thus,

$$Re_x^{\frac{1}{2}}C_f=2\left(\frac{m+3}{6}\right)^{1/2}\phi(t^*)(F_\eta)_w. \tag{10}$$

The local heat transfer rate at the wall in terms of Nusselt number can be expressed as

$$Re_x^{-\frac{1}{2}}Nu=-\left(\frac{m+3}{6}\right)^{1/2}(G_\eta)_w, \tag{11}$$

where $Nu=-\frac{[x(\frac{\partial T}{\partial y})]_w}{T_w-T_\infty}$.

## 3. Method of solution

The set of non-linear coupled partial differential equations (7) and (8) along with the initial conditions obtained from the corresponding steady state equations and boundary conditions (9) represent a non-linear two point boundary value problem for partial differential equations which is solved by an implicit finite difference scheme in combination with the quasilinearization technique [11,12]. Quasilinearization technique can be viewed as a generalization of the Newton–Raphson approximation technique in functional space. An iterative sequence of linear equations are carefully constructed to approximate the the non-linear Eqs. (7) and (8) for achieving quadratic convergence and monotonocity.

Applying quasilinearization technique [11,12], the non-linear coupled partial differential equations (7) and (8) are replaced by the following sequence of linear partial differential equations:

$$F^{i+1}_{\eta\eta} + X^i_1 F^{i+1}_{\eta} + X^i_2 F^{i+1} + X^i_3 F^{i+1}_{\xi} + X^i_4 F^{i+1}_{t^*} + X^i_5 G^{i+1} = X^i_6 \tag{12}$$

$$G^{i+1}_{\eta\eta} + Y^i_1 G^{i+1}_{\eta} + Y^i_2 G^{i+1}_{\xi} + Y^i_3 G^{i+1}_{t^*} + Y^i_4 F^{i+1} = Y^i_5 \tag{13}$$

The coefficient functions with iterative index $i$ are known and the functions with iterative index $i+1$ are to be determined. The boundary conditions become

$$\begin{aligned} &F^{i+1} = 0, \quad G^{i+1} = 1 \quad \text{at } \eta = 0, \\ &F^{i+1} = 1, \quad G^{i+1} = 0 \quad \text{at } \eta = \eta_\infty, \end{aligned} \tag{14}$$

where $\eta_\infty$ is the edge of the boundary layer. The coefficients in Eqs. (12) and (13) are given by

$$X^i_1 = \phi f + 2\left(\frac{m-3}{m+3}\right) t^* \left[\frac{\mathrm{d}\phi}{\mathrm{d}t^*} + \phi f_{t^*}\right] + \left(\frac{m}{3+m}\right)\phi\xi f_\xi,$$

$$X^i_2 = -2\left(\frac{2m}{m+3}\right)\phi F - \phi^{-1}\frac{\mathrm{d}\phi}{\mathrm{d}t^*} - 2\left(\frac{m-3}{m+3}\right) t^* \times \left[2\frac{\mathrm{d}\phi}{\mathrm{d}t^*}F + F_{t^*}\phi\right] - \left(\frac{3}{3+m}\right)\phi\xi F_\xi,$$

$$X^i_3 = -\left(\frac{3}{3+m}\right)\phi\xi F, \quad X^i_4 = -1 - 2\left(\frac{m-3}{m+3}\right) t^*\phi F,$$

$$X^i_5 = \frac{6}{m+3}\lambda\phi^{-1},$$

$$X^i_6 = -\left(\frac{2m}{m+3}\right)\phi(1+F^2) - \phi^{-1}\frac{\mathrm{d}\phi}{\mathrm{d}t^*} - 2\left(\frac{m-3}{m+3}\right) t^* \times \left[\frac{\mathrm{d}\phi}{\mathrm{d}t^*} + F^2 + \phi F F_{t^*}\right] - \left(\frac{3}{m+3}\right)\phi\xi F F_\xi,$$

$$Y^i_1 = Pr\left[\phi f + 2\left(\frac{m-3}{m+3}\right) t^* \left[\frac{\mathrm{d}\phi}{\mathrm{d}t^*} f + \phi f_{t^*}\right] + \left(\frac{3}{3+m}\right)\phi\xi f_\xi\right],$$

$$Y^i_2 = Pr\left[-\frac{3}{m+3}\phi\xi F\right], \quad Y^i_3 = -Pr\left[1 + 2\left(\frac{m-3}{m+3}\right) t^*\phi F\right],$$

$$Y^i_4 = -Pr\left[2\left(\frac{m-3}{m+3}\right) t^*\phi G_{t^*} - \left(\frac{3}{3+m}\right)\phi\xi G_\xi\right],$$

$$Y^i_5 = -Pr\left[2\left(\frac{m-3}{m+3}\right) t^*\phi F G_{t^*} - \left(\frac{3}{m+3}\right)\phi\xi F G_\xi\right].$$

Since the method is described for ordinary differential equations by Inouye and Tate [12] and also explained for partial differential equations in a recent article by Roy and Saikrishnan [13], it's detailed description is not presented here for the sake of brevity. In brief at each iteration step, the sequence of linear partial differential equations (12) and (13) were expressed in difference form using central difference scheme in the $\eta-$ direction and backward difference scheme in $\xi-$ and $t^*-$ directions. The resulting difference equations were then reduced to a system of linear algebraic equations with a block tri-diagonal structure which is solved by using Varga algorithm [14].

To ensure the convergence of the numerical solution to exact solution, the step sizes $\Delta\eta$, $\Delta\xi$ and $\Delta t^*$ have been optimized and the results presented here are independent of the step sizes at least upto the fourth decimal place. The step sizes $\Delta\eta$, $\Delta\xi$ and $\Delta t^*$ have been taken as 0.01, 0.02 and 0.01, respectively. A convergence criteria based on the relative difference between the current and previous iterative values of the velocity and temperature gradients at the wall are employed. When the difference reaches less than $10^{-4}$, the solution is assumed to have converged and the iterative process is terminated.

## 4. Result and discussion

Computations have been carried out for various values of $Pr(0.7 \leqslant Pr \leqslant 7.0)$, $\lambda(0 \leqslant \lambda \leqslant 7)$ and $A(-1.2 \leqslant A \leqslant 1.2)$. In all numerical computations $m$ is taken as $\frac{3}{2}$ and the edge of the boundary layer $\eta_\infty$ is taken between 3 and 5 depending on the values of parameters. The results have been carried out for both accelerating $(\phi(t^*) = 1 + \epsilon t^{*2}, \epsilon > 0, 0 \leqslant t^* \leqslant 1)$ and decelerating $(\phi(t^*) = 1 + \epsilon t^{*2}, \epsilon < 0, 0 \leqslant t^* \leqslant 1)$ free stream velocities of the fluid. In order to verify the correctness of the procedure, solutions have been obtained for the steady state case with $\xi = 0$, $\lambda = 0$ and $m = 0$ to compare the velocity and temperature profiles ($F$ and $G$) with those of Kumari et al. [6] for different values of Prandtl number, $Pr = 0.733$ and 6.7. Steady state results are also compared for various values of Prandtl numbers with those of Hering and Grosh [1], and Himasekhar et al. [2]. The results are found in an excellent agreement and only some of the comparisons are shown in Table 1 and in Fig. 2 to brief the manuscript.

The effects of buoyancy parameter $\lambda$, the axial distance $\xi$ and Prandtl number $Pr$ on velocity and temperature profiles ($F$,$G$) for accelerating flow $\phi(t^*) = 1 + \epsilon t^{*2}, \epsilon > 0$ are displayed in Figs. 3 and 4. Also, the effects of $\xi$ and $\lambda$ on the skin friction and heat transfer coefficients ($Re_x^{1/2} C_f$, $Re_x^{-1/2} Nu$) are presented in Fig. 5. The action of the buoyancy force shows the overshoot in the velocity profiles ($F$) near the wall for lower Prandtl number (air, $Pr = 0.7$) but for higher Prandtl number (water, $Pr = 7.0$) the velocity overshoot in $F$ is not observed as shown in Fig. 3. The magnitude of the overshoot increases with buoyancy parameter $\lambda$ but decreases with the increase of time $t^*$. The reason is that the buoyancy force ($\lambda$) effect is larger

Table 1
Comparison of the steady state skin friction and heat transfer parameter results ($f''(0)$, $-G'(0)$) with those of Hering and Grosh [1] and Himasekhar et al. [2] for $m = 0$

| $Pr$ | $\lambda$ | Himasekhar et al. [2] | | Present results | |
|---|---|---|---|---|---|
| | | $-G'(0)$ | $f''(0)$ | $-G'(0)$ | $f''(0)$ |
| 0.7 | 1.0 | 0.6120 | 2.2012 | 0.6125 | 2.2019 |
| | | | | 0.6120[a] | 2.2078[a] |
| | 10 | 1.0097 | 8.5041 | 1.0105 | 8.5049 |
| | | | | 1.0173[a] | 8.5246[a] |
| 1 | 1.0 | 0.7010 | 2.0886 | 0.7015 | 2.0901 |
| | 10 | 1.1230 | 7.9425 | 1.1294 | 7.9445 |
| 10 | 1.0 | 1.5662 | 1.5636 | 1.5785 | 1.5658 |
| | 10 | 2.3580 | 5.0821 | 2.3587 | 5.0861 |

[a] Values taken from Hering and Grosh [1].

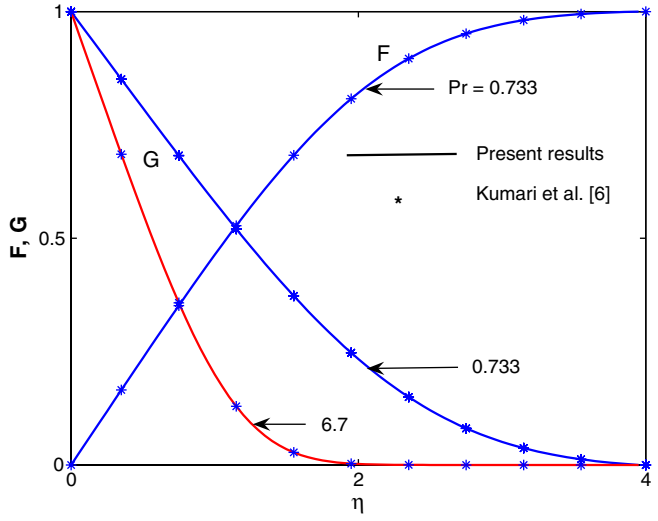


Fig. 2. Comparison of velocity and temperature profiles (F, G) with those of Kumari et al. [6] when $\xi = 0$, $\lambda = 0$ and $m = 0$.

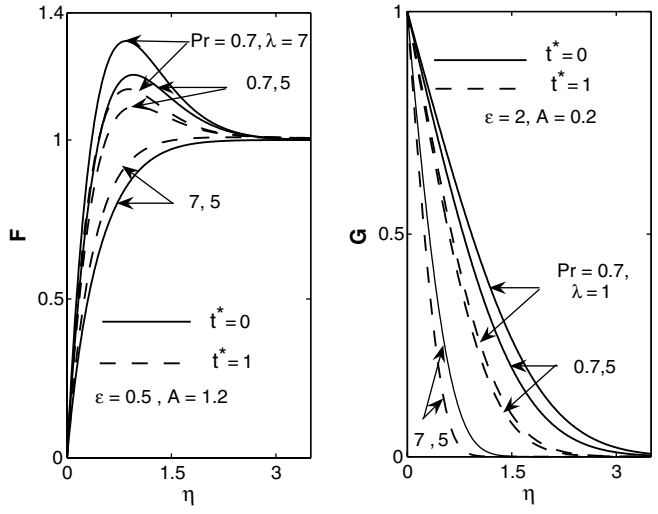


Fig. 3. Effects of $\lambda$ and $Pr$ on $F$ and $G$ for $\phi(t^*) = 1 + \epsilon t^{*^2}$ at $\xi = 0.5$ when $m = \frac{3}{2}$.

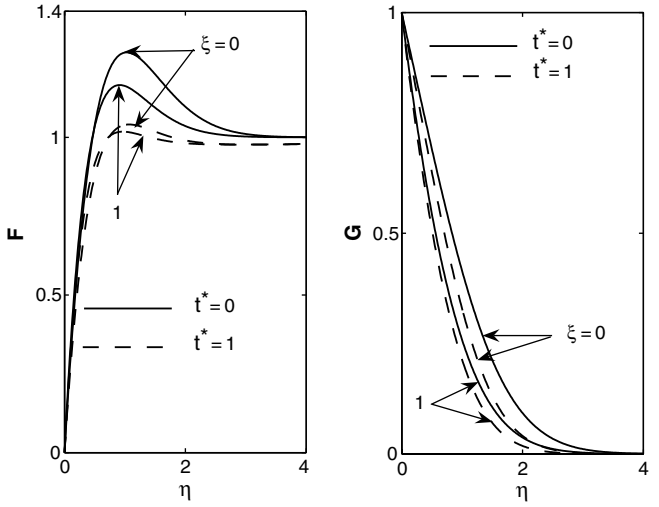


Fig. 4. Effect of $\xi$ on $F$ and $G$ for $\phi(t^*) = 1 + \epsilon t^{*^2}, \epsilon = 1.0$ when $Pr = 0.7$, $A = 1$, $\lambda = 5$ and $m = \frac{3}{2}$.

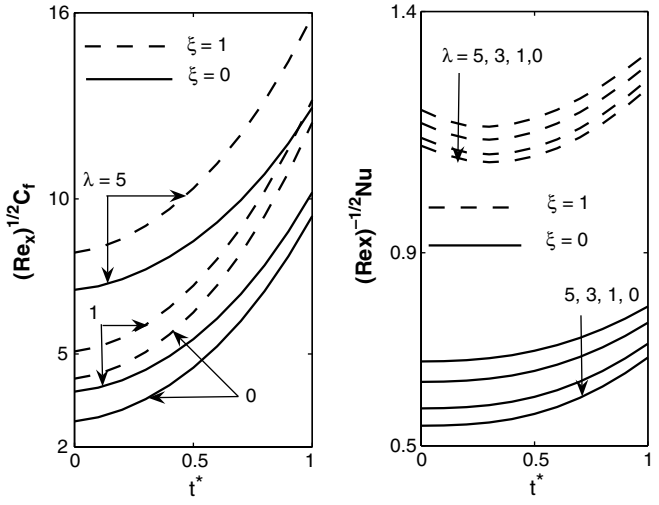


Fig. 5. Effects of $\lambda$ and $\xi$ on $Re_x^{1/2}C_f$ and $Re_x^{-1/2}Nu$ for $\phi(t^*) = 1 + \epsilon t^{*^2}$, $\epsilon = 1$ when $Pr = 0.7$, $A = 1$ and $m = \frac{3}{2}$.

for $Pr = 0.7$ (air) due to low viscosity of the fluid which enhances the velocity within the boundary layer as the assisting buoyancy force acts like a favorable pressure gradient and the velocity overshoot occurs. For $Pr = 7.0$ (water) the velocity overshoot is not present because water is more viscous fluid which makes it less sensitive to the buoyancy parameter $\lambda$. The effect of $\lambda$ is comparatively less on the temperature profiles ($G$) as shown in Fig. 3. Moreover, Fig. 3 shows that the increase of Prandtl number $Pr$ results into thinner thermal boundary layer as the higher Prandtl number fluid has a lower thermal conductivity.

Fig. 4 shows that due to the increase in axial distance $\xi$, the steepness in both the velocity and temperature profiles ($F, G$) near the wall increases and consequently reduce the thicknesses of both the velocity and thermal boundary layers. Further, it may be pointed out that the magnitude of the velocity overshoot slightly decreases with the increase

of $\xi$ as can be seen in Fig. 4. Thus for the increase of $\xi$ i.e., at a distant axial location, the effect of buoyancy parameter $\lambda$ on velocity profiles ($F$) is small so that it does not cause the velocity profiles to increase the magnitude of overshoots further in buoyancy aided flows. For all the cases both the profiles ($F$,$G$) at a later time $t^* = 1$ are comparatively more steeper near the wall than those at the initial time $t^* = 0$, which can be seen in Figs. 3 and 4. Results presented in Fig. 5 indicates that the skin friction and heat transfer coefficients ($Re_x^{1/2}C_f, Re_x^{-1/2}Nu$) increase with the increase of buoyancy parameter ($\lambda$). The physical reason is that the positive buoyancy force ($\lambda$) implies favorable pressure gradient and the fluid gets accelerated which results in thinner momentum and thermal boundary layers. Consequently, the skin friction ($Re_x^{1/2}C_f$) and the Nusselt number ($Re_x^{-1/2}Nu$) also increase with the increase of $\lambda$ at any time ($t^*$) as shown in Fig. 5. For example for $Pr = 0.7$, $A = 1$ at time $t^* = 0.5$, Fig. 5 shows that the percentage increase in $Re_x^{1/2}C_f$ and $Re_x^{-1/2}Nu$ for the increase of $\lambda$ from 1 to 5 are, approximately, 43.54% and 5.4%, respectively.

The effect of surface mass transfer parameter $A$ ($A > 0$ or $A < 0$) on the velocity and temperature profiles ($F$,$G$) for $\phi(t^*) = 1 + \epsilon t^{*^2}$, $\epsilon = 0.5$, $Pr = 0.7$ and $\xi = 1$ are presented in Fig. 6. In addition, Fig. 7 displays the effect of $A$ on skin friction and heat transfer coefficients ($Re_x^{1/2}C_f$, $Re_x^{-1/2}Nu$) with the increase of time $t^*$ from 0 to 1. Fig. 7 shows that for all time $t^*$, both skin friction and heat transfer coefficients ($Re_x^{1/2}C_f$, $Re_x^{-1/2}Nu$) increase with suction ($A > 0$) but decrease with the increase of injection ($A < 0$). In case of injection, the fluid is entered into the boundary layer from the surface causing reduction in velocity gradient as it tries to maintain the same velocity over a very small region near the surface and the effect is reverse in case of suction. For example, for $Pr = 0.7$, $\xi = 1$ at $t^* = 0.5$ both the $Re_x^{1/2}C_f$ and $Re_x^{-1/2}Nu$ increase, approximately, by 33.1% and 86.07%, respectively, with the increase of

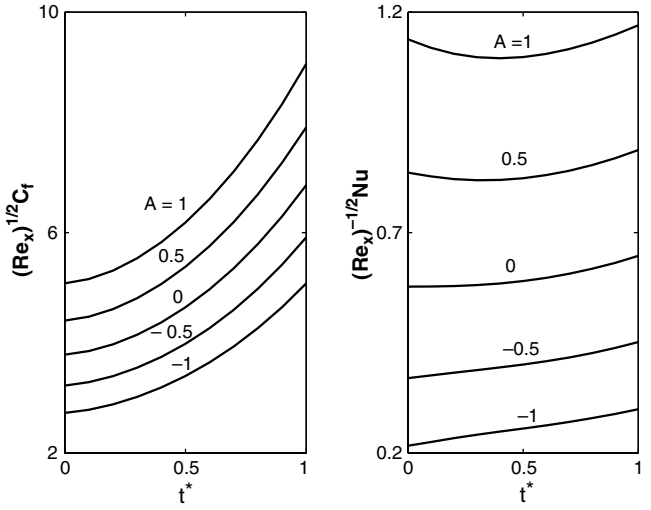


Fig. 7. Effect of $A$ on $Re_x^{1/2}C_f$ and $Re_x^{-1/2}Nu$ for $\phi(t^*) = 1 + \epsilon t^{*^2}$, $\epsilon = 0.5$ when $Pr = 0.7$, $\xi = 1$, $\lambda = 1$ and $m = \frac{3}{2}$.

suction from $A = 0$ to $A = 1$. On the other hand, for $Pr = 0.7$, $\xi = 1$ at $t^* = 0.5$ due to increase of injection from $A = 0$ to $A = -1$ both the $Re_x^{1/2}C_f$ and $Re_x^{-1/2}Nu$ decrease 26.81% and 59.66%, respectively. The graphs of the velocity and temperature profiles ($F$,$G$) versus $\eta$ in Fig. 6 show that the injection ($A < 0$) causes a decrease in the steepness of the profiles $F$ and $G$ near the wall but steepness of the profiles ($F$,$G$) increase with suction.

Fig. 8 displays the effect of Prandtl number for accelerating and decelerating free stream flows ($\phi(t^*) = 1 + \epsilon t^{*^2}$, $\epsilon = 0.5$ and $\epsilon = -0.5$) on the skin friction and heat transfer coefficients ($Re_x^{1/2}C_f, Re_x^{-1/2}Nu$) where $\lambda = 4$, $\xi = 0.5$ and $A = 0$. It is found from Fig. 8 that the skin friction coefficient decreases with increase of Prandtl number because the higher Prandtl number fluid (water, $Pr = 7.0$) means more viscous fluid which increases the boundary layer thickness and consequently reduce the shear stress. On the other

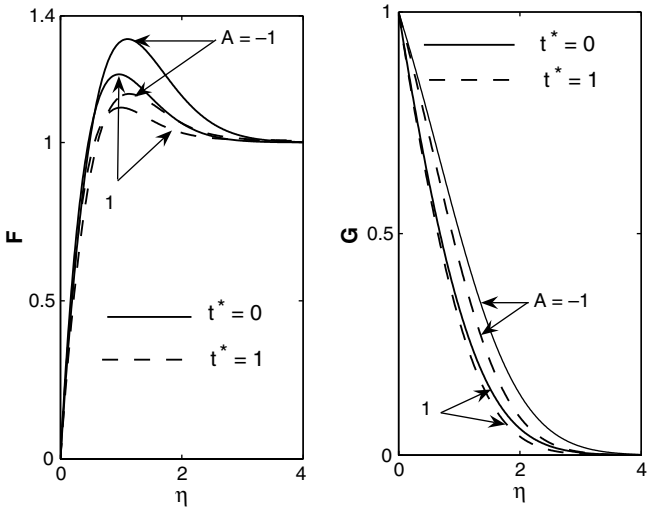


Fig. 6. Effect of $A$ on $F$ and $G$ for $\phi(t^*) = 1 + \epsilon t^{*^2}, \epsilon = 0.5$ when $\lambda = 5$, $Pr = 0.7$, $\xi = 1.0$ and $m = \frac{3}{2}$.

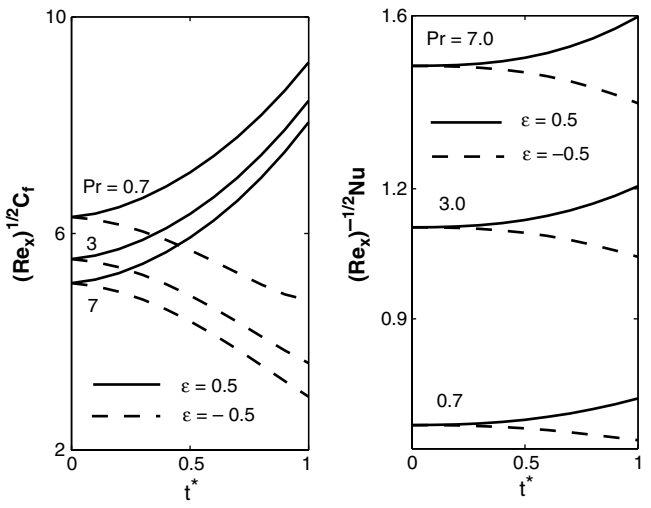


Fig. 8. Effects of $Pr$ and $\epsilon$ on $Re_x^{1/2}C_f$ and $Re_x^{-1/2}Nu$ for $\phi(t^*) = 1 + \epsilon t^{*^2}$ when $\xi = 0.5$, $A = 0$, $\lambda = 4$ and $m = \frac{3}{2}$.

hand, Fig. 8 reveals that the surface heat transfer rate increases significantly with Pr as $Pr = 7$ has a lower thermal conductivity which results in thinner thermal boundary layer (see Fig. 3 for temperature profile G) and hence a higher heat transfer rate at the wall. To be more specific for $\lambda = 4$ at $t^* = 0.5$, as $Pr$ increases from 0.7 to 7.0, $Re_x^{1/2} C_f$ decreases by about 16.89% and $Re_x^{-1/2} Nu$ increases by 125.36%, respectively, for accelerating flow. Thus, the heat transfer rate at the wall can be reduced by using a low Prandtl number fluid such as air ($Pr = 0.7$). In case of accelerating flow, Fig. 8 shows that both skin friction and heat transfer coefficients ($Re_x^{1/2} C_f$, $Re_x^{-1/2} Nu$) increase with time $t^*$ and the effect of the time variation is found to be more pronounced on the skin friction coefficient than on heat transfer rate, because the change in the free stream velocity with the time strongly affects the velocity component. For example, for $Pr = 7.0$ the values of $Re_x^{1/2} C_f$ and $Re_x^{-1/2} Nu$ increase by about 58.43% and 7.64%, respectively, when the time $t^*$ increases from 0 to 1. In contrast, both $Re_x^{1/2} C_f$ and $Re_x^{-1/2} Nu$ decrease with time $t^*$ for the case of decelerating flow as seen in Fig. 8. In particular for $Pr = 7.0$, the values of $Re_x^{1/2} C_f$ and $Re_x^{-1/2} Nu$ decrease by about 41.29% and 5.83%, respectively, with the increase of time $t^*$ from 0 to 1.

## 5. Conclusions

Non-similar solution of an unsteady mixed convection flow over a vertical cone has been obtained for both accelerating and decelerating free stream velocities. The results pertaining to the present study indicate that the skin friction coefficient is significantly affected by the time dependent free stream velocity distributions whereas the heat transfer coefficient is comparatively little affected by it. It is found that the buoyancy force ($\lambda$) enhances the skin friction coefficient and Nusselt number. In the buoyancy aiding flow ($\lambda > 0$), the velocity profiles exhibit velocity overshoot for lower Prandtl number. Further, the buoyancy parameter ($\lambda$) and injection parameter ($A < 0$) tend to increase its magnitude but the suction parameter ($A > 0$) and axial distance $\xi$ tend to reduce the magnitude of the velocity overshoot. For a fixed buoyancy force, the Nusselt number increases with Prandtl number but the skin friction coefficient decreases. In fact, the increase in Prandtl number causes a significant reduction in the thickness of thermal boundary layer. As expected, both skin friction and heat transfer coefficients increase with suction but decrease with the increase of injection. Moreover, it is noted that the suction parameter ($A > 0$) and the axial distance steepen both the velocity and temperature profiles, but injection ($A < 0$) does the reverse.

## References

[1] R.G. Hering, R.J. Grosh, Laminar combined convection from a rotating cone, ASME J. Heat Transfer 85 (1963) 29–34.
[2] K. Himasekhar, P.K. Sarma, K. Janardhan, Laminar mixed convection from a vertical rotating cone, Int. Comm. Heat Mass Transfer 16 (1989) 99–106.
[3] C.Y. Wang, Boundary layer on a rotating cones, disc, axisymmetric surfaces with concentrated heat sources, Acta. Mech. 81 (1990) 245–251.
[4] D. Anilkumar, S. Roy, Unsteady mixed convection flow on a rotating cone in a rotating fluid, Appl. Math. Comput. 155 (2004) 545–561.
[5] S. Roy, D. Anilkumar, Unsteady mixed convection from a rotating cone in a rotating fluid due to combined effects of thermal and mass diffusion, Int. J. Heat Mass Transfer 47 (2004) 1673–1684.
[6] M. Kumari, I. Pop, G. Nath, Mixed convection along a vertical cone, Int. Comm. Heat Mass Transfer 16 (1989) 247–255.
[7] K.A. Yih, Mixed convection about a cone in a porous medium: the entire region, Int. Comm. Heat Mass Transfer 26 (1999) 1041–1050.
[8] H. Schlichting, Boundary Layer Theory, Springer, 2000, pp. 86–89.
[9] I. Pop, D.B. Ingham, Convective Heat Transfer: Mathematical and Computational Modelling of Viscous Fluids and Porous Media, Pergaman, Oxford, 2001.
[10] A. Bejan, Convective Heat Transfer, Wiley Interscience, 1994.
[11] R.E. Bellman, R.E. Kalaba, Quasilinearization and Non-linear Boundary Value Problems, American Elsevier Publishing Co. Inc., New York, 1965.
[12] K. Inouye, A. Tate, Finite difference version of quasilinearization applied to boundary layer equations, AIAA J. 12 (1974) 558–560.
[13] S. Roy, P. Saikrishnan, Non-uniform slot injection (suction) into steady laminar boundary layer flow over a rotating sphere, Int. J. Heat Mass Transfer 46 (2003) 3389–3396.
[14] R.S. Varga, Matrix Iterative Analysis, Prentice-Hall, 2000.